Hydrocarbon Reservoirs Study of Abu Roash G and Bahariya Formations at Bahga Field in Alam El-Shawish Concession, North Western Desert, Egypt

Hassan H. El-kadi[1], Hassan M. El-Shayeb[2], M.Fathy[1], Ahmed A.K. Elnashar[1]

[1]Geology Department, Faculty of Science, Al-Azhar University, Cairo, Egypt.
[2]Geology Department, Faculty of Science, Menoufiya University, Egypt.
a_nashar88@yahoo.com

Abstract: Bahga field lies in the central part of the Alam El-Shawish West (AESW) concession which is located in the northern part of the Western Desert. The aim of this study is to evaluate the subsurface geological system and hydrocarbon potentialities of Late Cretaceous reservoirs for Abu Roash (AR/G) and Bahariya (BAH) by combine the different available data of electiric logs and seismic for seven wells at Bahga field. Petrophysical analysis has been established on the available wells within the study area by using electric logs (Gamma Ray tool (GR), Resistivity tool of Array Induction tool (AIT), Density tool (RHOB), Neutron Porosity tool (NPHI), Sonic tool (DT), Photo Electric tool (PEF)) to determine the reservoir properties such as (facies, clay volume, water saturation, effective porosity and reservoir net thickness). Seismic interpretation was establish on the available seismic section concerned with the study area to provide a detailed structural interpretation to determine the structural geometry of AR/G and Bahariya Reservoirs for detecting the best localities for drilling new development wells within the study area. The structure contour maps and the 3D structural model confirm the field consists of a three-way-dip-fault closure at top AR/G level. However, only a limited crestal portion covering 4km x 1km area is hydrocarbon bearing. The field is an elongated NW-SE oriented 2 ways closed structure bounded by high angle NW-SE trending normal faults. Additional smaller scale normal faults parallel to the main bounding faults may result in local fault block compartmentalization. 3D static model using structure model and well log data have been done for proper optimization and development of hydrocarbon potential at Bahga field. Seismic data were used to generate the input interpreted horizon grids and fault modeling of the structure model. Property modeling (facies, effective porosity, and water saturation) was distributed and mapped within the constructed 3D grid using deterministic Kriging algorithms while facies were distributed and mapped by deterministic facies modeling method. Based on the current work another promising area was determined for promised development plans to reach the highest and best commercial cases.

[Hassan H. El-kadi, Hassan M. El-Shayeb, M.Fathy, Ahmed A.K. Elnashar. **Hydrocarbon Reservoirs Study of Abu Roash G and Bahariya Formations at Bahga Field in Alam El-Shawish Concession, North Western Desert, Egypt.** *N Y Sci J* 2017;10(12):44-63]. ISSN 1554-0200 (print); ISSN 2375-723X (online). http://www.sciencepub.net/newyork. 6. doi:10.7537/marsnys101217.06.

Keywords:- Hydrocarbon Reservoirs Study of Abu Roash G and Bahariya Formations by combin different data of eclectric logs and seismic data at Bahga Field, North Western Desert, Egypt

1. Location of the Study Area

The Bahga field is located in the north western desert of Egypt approximately 300 Km to the South West of Cairo, lies in the center of the AESW concession (Figure 1).

2. Field Overview

The field was discovered in February 2007 with the drilling of Bahga 1 well. Currently the field is penetrated by twelve wells. Two hydrocarbon oil reservoirs are encountered in the Bahga field; Abu Roash-G (AR/G), Bahariya (BAH). Only six wells encountered hydrocarbon pay sands in the AR/G reservoir (Bahga 1, 4, 5, 6, 10 & 11) which are all concentrated in the East of the field outline. Only five wells encountered hydrocarbon pay sands in the Bahariya & Kharita reservoir (Bahga 3, 7, 8, 9, & C101).

The subsequent drilled wells from Bahga 2 to Bahga 8 confirmed that the accumulation consists of three separate hydro carbon bearing sequences; AR/G 1, AR/G 3, L. BAH.

AR/G 1 reservoir is only seen and produced in two wells Bahga 5 and Bahga 6. Both wells are not in pressure communication.

AR/G 3 reservoir is being produced by two wells Bahga 4 and Bahga 1 which is producing commingled from three different reservoirs.

L. Bah reservoir is discovered (March 2010) by well Bahga 7, Bahga 3 and Bahga 9.

3. Subsurface Geological Setting

3.1. Stratigraphic Framework

The lithostratigraphic column of the Abu Gharadig basin comprises rock units ranging from Cambrian to Recent with the oldest sediments resting

non-conformably on the basement rocks [El Ayouty 1990]. In the Abu Gharadig basin, the sedimentary column reaches between 8 to 9 km [Hantar 1990]. The generalized stratigraphic sequence show in (Figure 2).

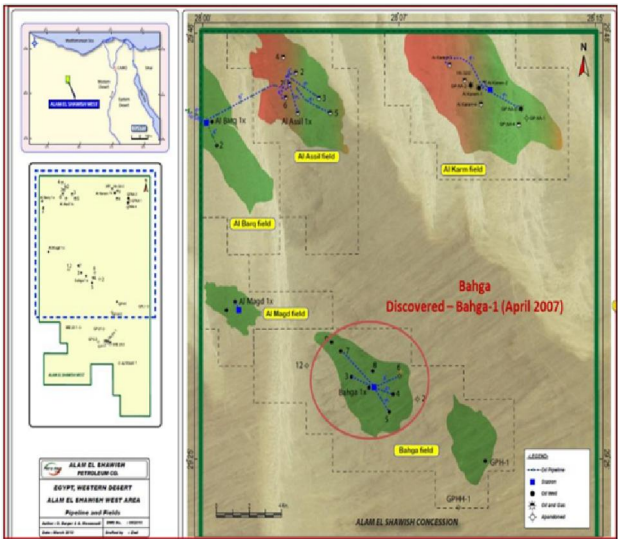

Fig. 1.1: Alam El Shawish Concession Map

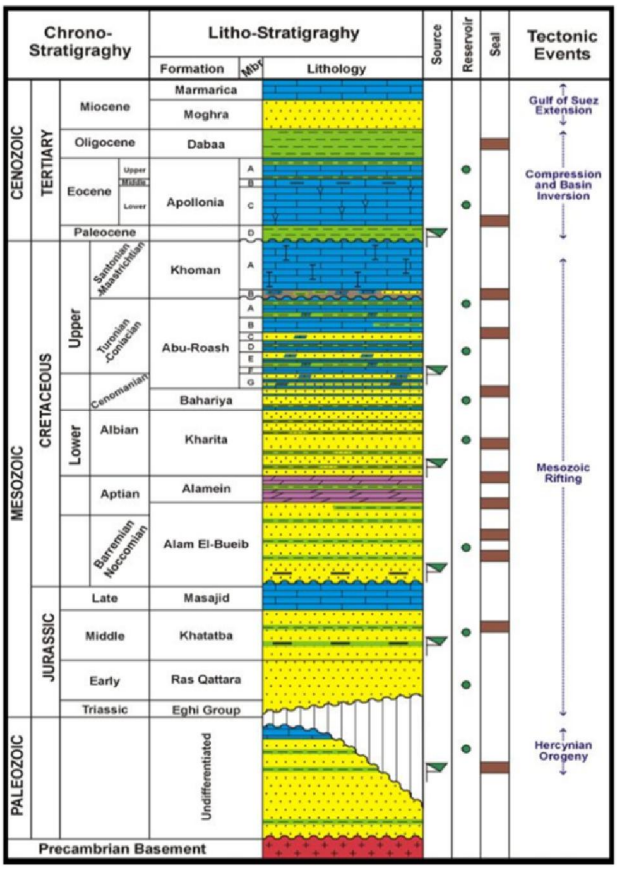

Fig. 2: Generalized Stratigraphic Column of the North Western Desert of Egypt. (Moustafa, et al.2003

3.2. Structure and Tectonic Settings

The dominant structural style of the Western Desert comprises two systems: a deeper series of low-relief horst and graben belts, separated by master faults of large throw, and broad Late Tertiary folds at shallower depth [Sestini 1984].

Abu Gharadig basin is a rift basin bounded to the north and south by two right-lateral shears and from the east and west by northwest trending normal faults [Meshref 1990]. It was formed during the Albian, reached maximum subsidence in the Late Cretaceous (Maastrichtian) and was subsequently inverted during the Paleocene-Eocene [Lüning et al. 2004]. It seems to be a continuous basin with a major uplift along its center that divides it into north Abu Gharadig Basin and south Abu Gharadig Basin [Meshref 1990]. The structural pattern of Abu Gharadig Basin is dominated by NE-SW oriented faults coupled with a strong pattern of NW–SE conjugate faults. These fault patterns suggest regional wrench movement [Abd El Aal 1988]. This in turn subdivided the basin into several structural units of varying importance named from E to W: the Mubarak High, the Abu Gharadig Anticline and the Mid Basin Arch [Meshref 1990]. (Figuer 3).

4. Seismic Interpretation and 3d Structure Modeling

4.1 Seismic Interpretation

Our available data in this study is 12 in-lines and 10 cross-lines of seismic sections (Figure 4) with the intention to produce a dense spatial interpretation, for better horizon /surface and faults evaluation needed to build 3D structure modeling the reservoir.

These interpretations and modeling that will guide us to the best localities for drilling development wells.

4.1.1. Picking Horizons and Faults

The manual seismic interpretation of horizons and faults was performed for reservoir sections. The seismic interpretation was set for interpretation for 12 in-lines and 10 cross-line traces with the intention to produce a dense spatial interpretation, for better horizon /surface evaluation needed for modeling the reservoir surfaces.

Manual interpretation is done by petrel software for one horizon AR/G. Bahariya and Kharita was mapped by isochoring down from the AR/G level and adjusting and extending the horizons at the fault breaks.

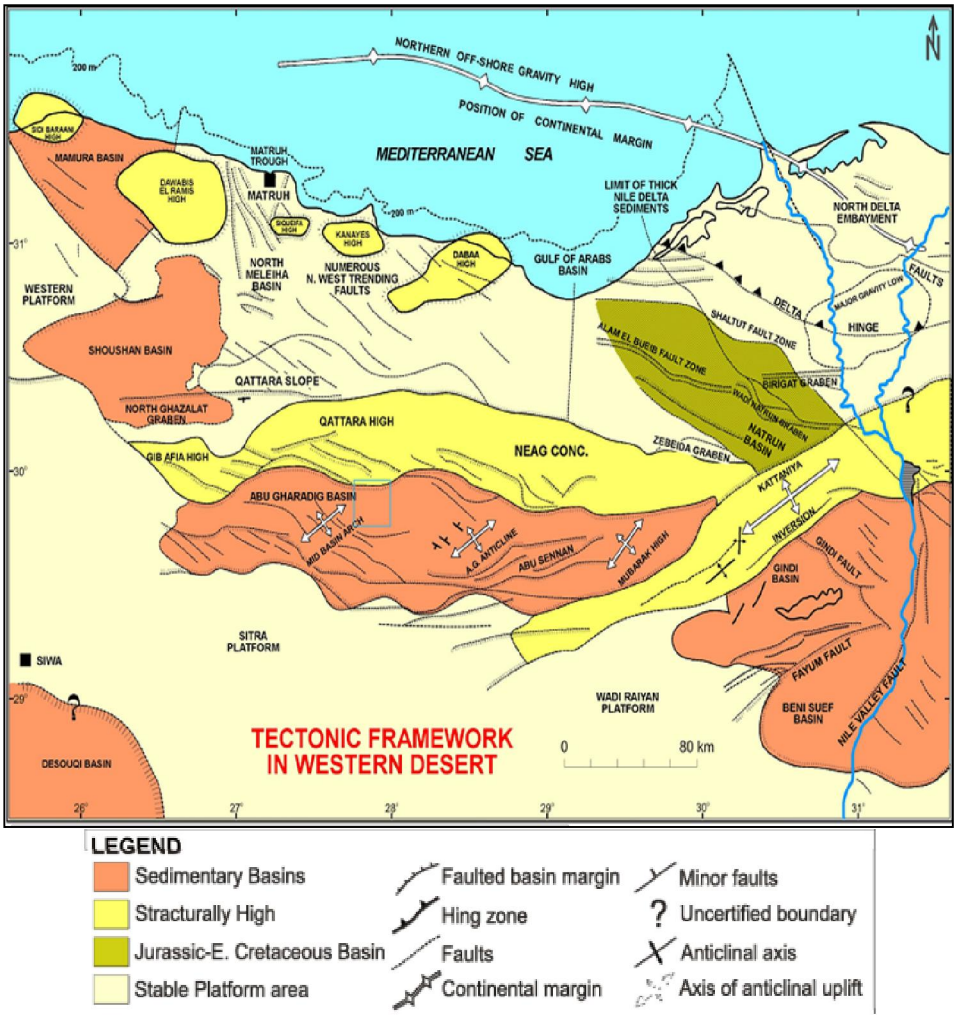

Fig. 3: 2-Dimensional Index Map Showing the Spatial Distribution of the Main East-West Sedimentary Basin and Major Tectonics in the North Western Desert, Egypt, Modified After [Bayoumi 1996].

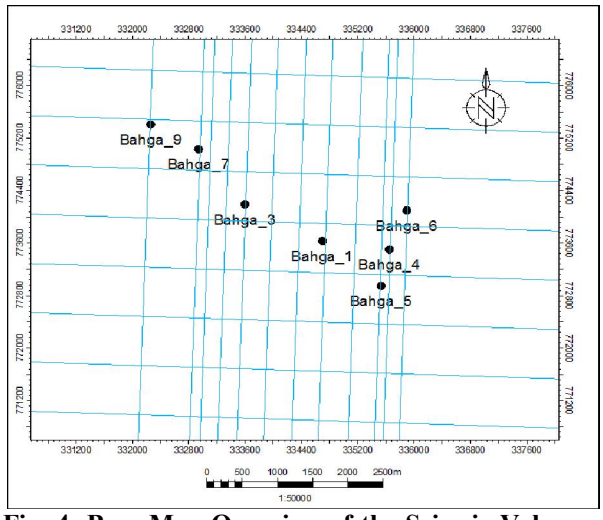

Fig. 4: Base Map Overview of the Seismic Volume, Capturing 12 Inlines And 10 Cross Lines at Bahga Field.

The process of generating the faults manually starts by having firm geologic interpretations of the faults, understanding their nature (whether they are planar, listric etc.) and the type of faults. In the Bahga seismic volumes the faults are manually picked within each seismic in-lines and cross-lines in the reservoir sections of the Bahga seismic volumes. In the seismic Interpretation window in Petrel, the Interpret fault tab is activated and fault interpretation folder is created where all the interpreted faults are stored, the manual point mode is used to interpret the length and trend of the fault (Figure 5).

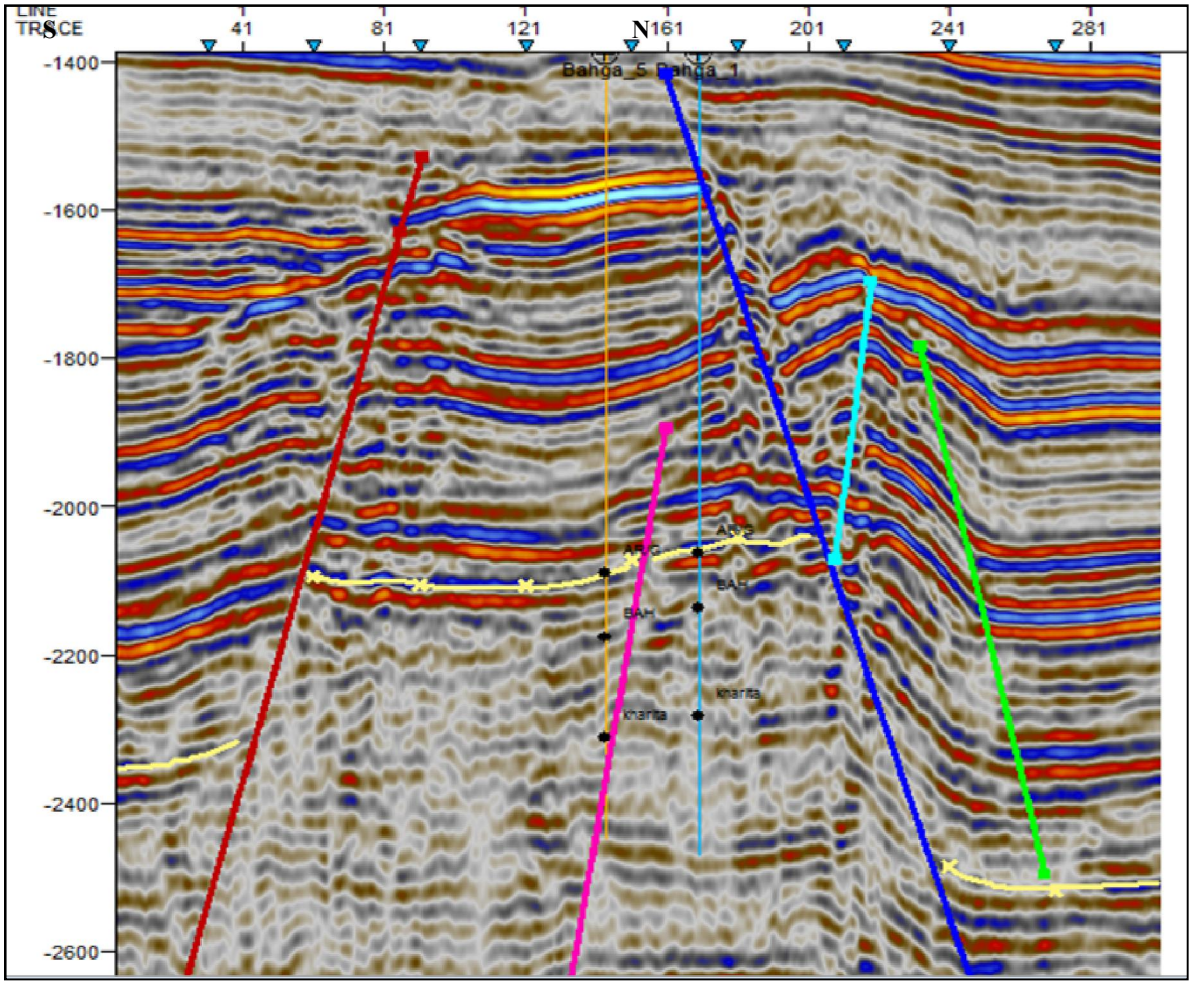

Fig. 5: Seismic Line (L2479) Showing the Manually Interpreted Horizons and Faults in the Seismic Interpr tation Window.

4.2 Structure Contour Maps

The construction of the seismic maps was followed by its interpretation, which is the explanation of the seismic data in terms of subsurface geologic information; otherwise the most important approach for petroleum exploration is to locate new prospects on the time and structure contour maps to be tested by drilling.

In the present study, the 2D-seismic lines are obtained in time domain. The interpretation of seismic line integrated with geological cross-sections to construct one time structural contour map then converted to depth contour map. These map are constructed at tops of horizons of Abu Roash "G" Member and isochored down depth to Upper and Lower Bahariya Members and top Kharita formation Generally these maps (Fig. 6) show a set of major normal faults (F1, F2). The main faults affect the Lower and Upper Cretaceous sequences trending northwest southeast and dipping towards the north-northeast, south-southwest and west directions. These faults are normal faults forming small horst between F1, F2 producing traps. The constructed depth structure contour map covers large area of Bahga field (12 x 3.5 km).

4.3. 3D Structure Modeling

Structure modeling is the first step in building the 3D modeling and is subdividing into three processes:

4.3.1 Fault Modeling

The fault modeling process is done by applying manual based techniques of isolating faults by interpreting fault zones of interest in the seismic sections which are correspondingly used to create 3D grid needed in the model.

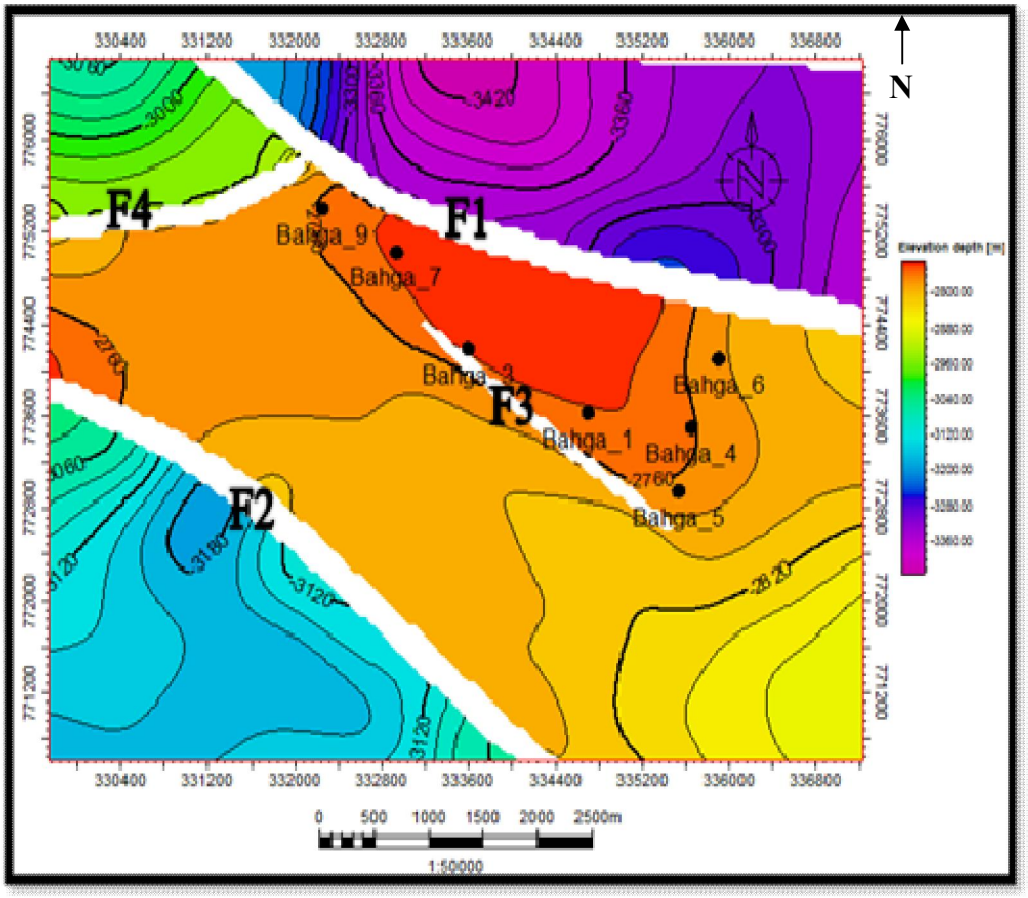

Fig. 6: Depth Structure Contour Map of Upper AR/G Member

4.3.2. Pillar Gridding

The process of fault modeling leads to fault gridding which is called pillar gridding, which represents the faults in a 3D grid system. The interpreted fault polygons in the fault interpretation folder are converted to fault sticks and polygons. This process converts the interpreted faults from the fault modeling workflow into pillars in 3D structural grid surface or model frame.

4.3.3. Vertical Layering

The vertical layering is the last process of building the 3D grid and is defined in three process steps:

-Make Horizons

Normally, the seismic interpretation is used to define the main vertical architecture of the reservoir model. When introducing the horizons to the set of pillars generated in the Pillar gridding process, all intersections between the pillars and the horizons become nodes in the 3D grid.

-Make Zones

The Make Zone process proved relevant in differentiating each of the reservoir tops into their corresponding reservoir zones. Zones can be added to models by thickness data in the form of isochores, constant thickness and percentages.

-Layering

Layering is defined as the internal layering reflecting the geological deposition of a specific zone. Layers only sub-divide the grid between the zone-related horizons. So The Layering process enables you to define the final vertical resolution of the grid by setting the cell thickness or the number of desired cell layers.

Finally, 3D structure modeling consists of fault modeling, pillar gridding and vertical layering (Figure 7). All three operation processes are tied together in one single data model (3D grid).

4.4 Structure Cross Section

Figure (8) illustrates the NW-SE structural cross section. It is located at the central part of the study area and shows that the area is affected by set normal faults forming a horst and graben blocks. Fault 1 is directed towards the NW-SE trend and its downthrown side is directed towards the NW trend. Fault 2 is also directed towards the NW-SE trend and its downthrown side is directed towards the SW trend.

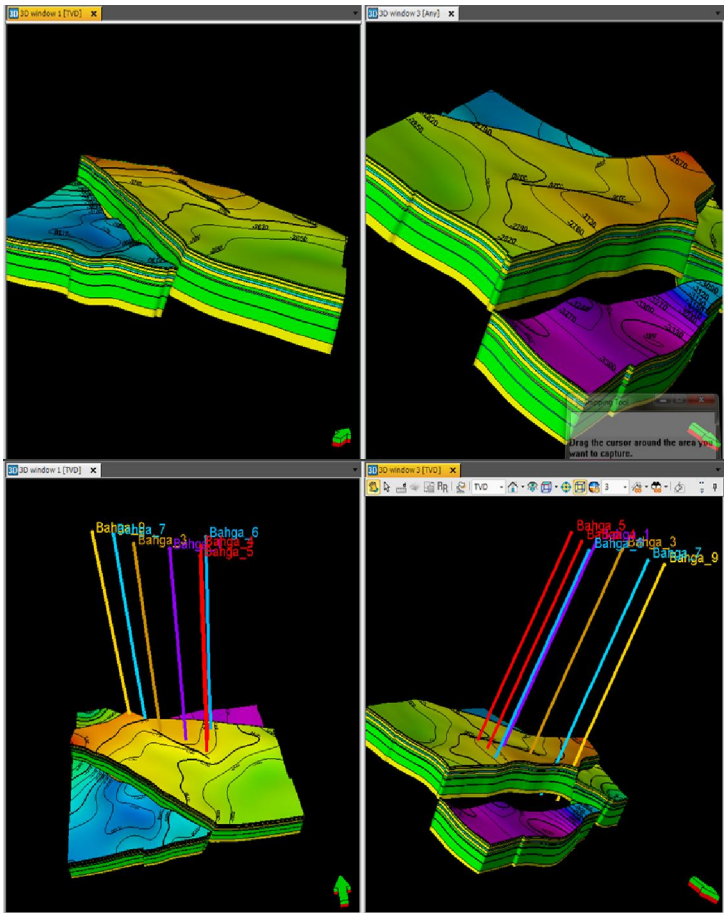

Fig 7: 3D Structure Model of Bahga Field Showing Horizons, Zones and Vertical Layers.

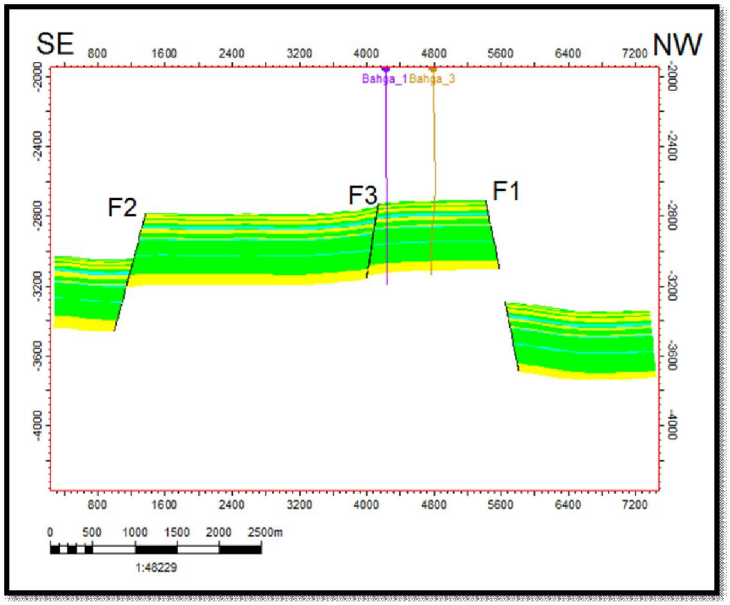

Fig 14: NW-SE structural Cross Section.

5. Well Log Analysis

The well logging deduced parameters, resulted from the application of formation evaluation program (TechLog Software), in addition to the corrected input-data, are presented level-wise in two vertical cross-plots, of the same depth scale, for each rock unit in

each well. This is in order to evaluate the hydrocarbon potentialities of the studied interval on the light of the petrophysical and lithological parameters achieved for each well individually.

In order to illustrate the vertical distribution of hydrocarbon saturation through petrophysical parameters, a number of litho-saturation cross-plots were constructed. These plots exhibit a number of continuous logs showing the variations inherited in rocks materials and parameters against depth.

5.1. Lithology Identification.

5.1.1 Di-Porosity Cross Plots

The neutron-density cross plot of AR/G1,2,3 and L-BAH RES of wells_1,4,5,6,3,7,9 (Figures 8,9) found that the majority of points overlie sandstone line and found that the points around sandstone line and limestone line in addition shows the same clay effect on the plotted data to the bellow right side of the plot.

Neutron-Density Cross-plots indicate that the main component of AR/G and L-BAH formation is Sandstone with little a mounts of limestone and dolomite which represent the calcareous cement.

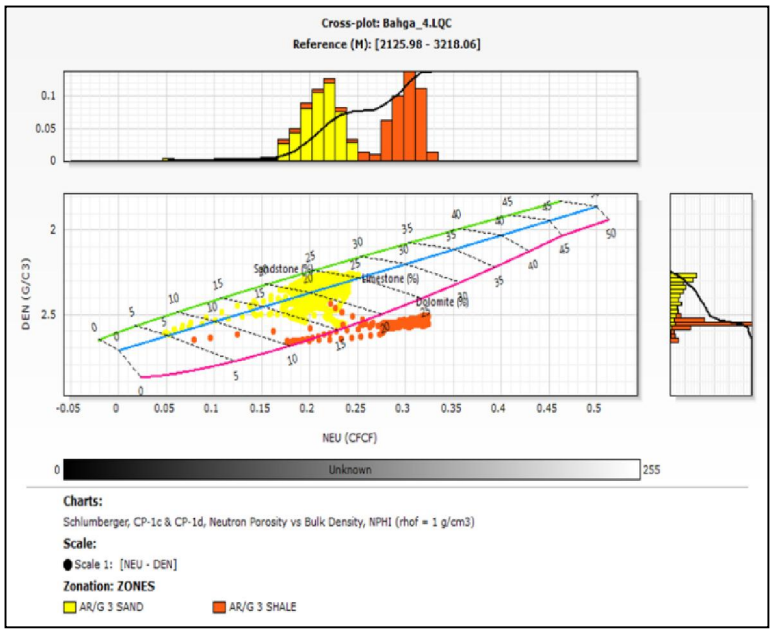

Fig. 8: Neutron-Density Cross Plot of Bahga 4, AR/G 3.

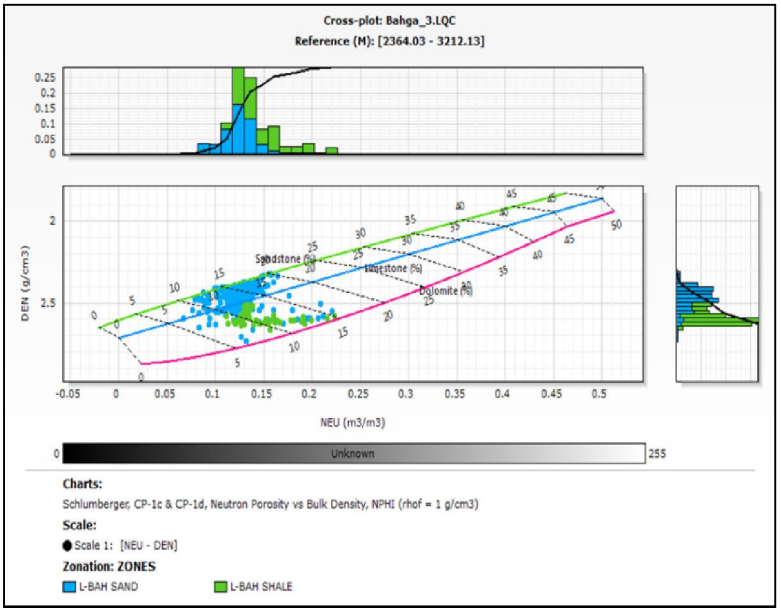

Fig. 9: Neutron-Density Cross Plot of Bahga 3, L-BAH.

5.1.2 Tri-Porosity (M-N) Cross Plots

The M-N plots depend on the fluid and log parameters, which are incorporated together essentially in the three porosity logs (ρb, ΔT and ΦN). From these, two functions M and N are calculated, which are independent of the primary porosity. Therefore, cross plotting of these two quantities help for defining the lithology characteristics more obviously (Schlumberger, 1987).

M-N (Tri-Porosity) Cross-plot indicates that the main component of AR/G 1, AR/G 3 and L-BAH formation is Sandstone represented by Quartz mineral with calcareous cement represented by Calcite and Dolomite minerals (Figures 10,11).

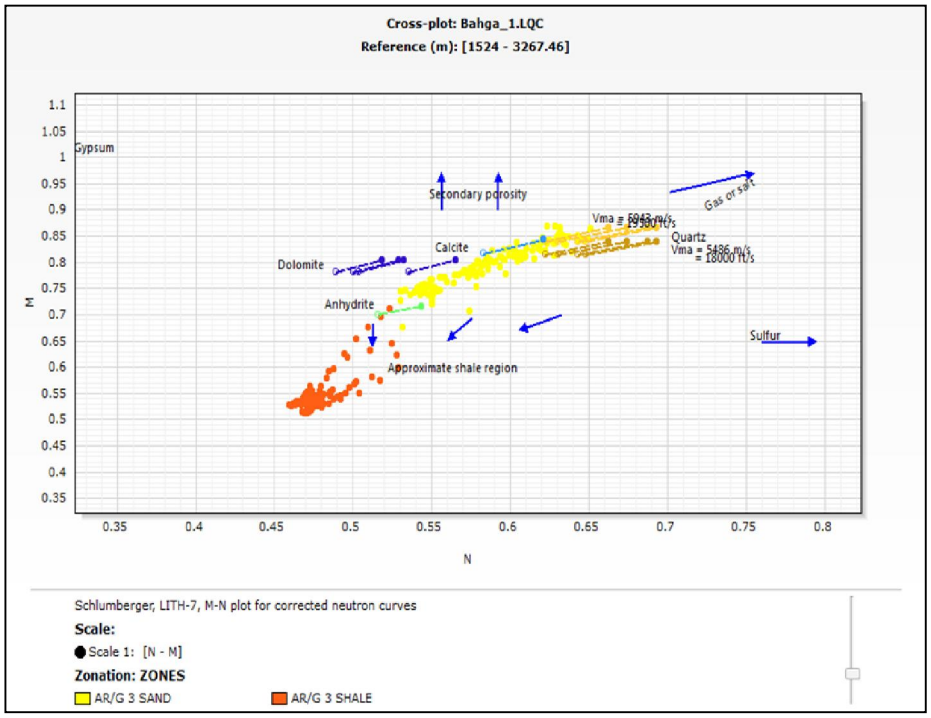

Fig. 10: M-N Cross Plot of Bahga 1, ARG 3.

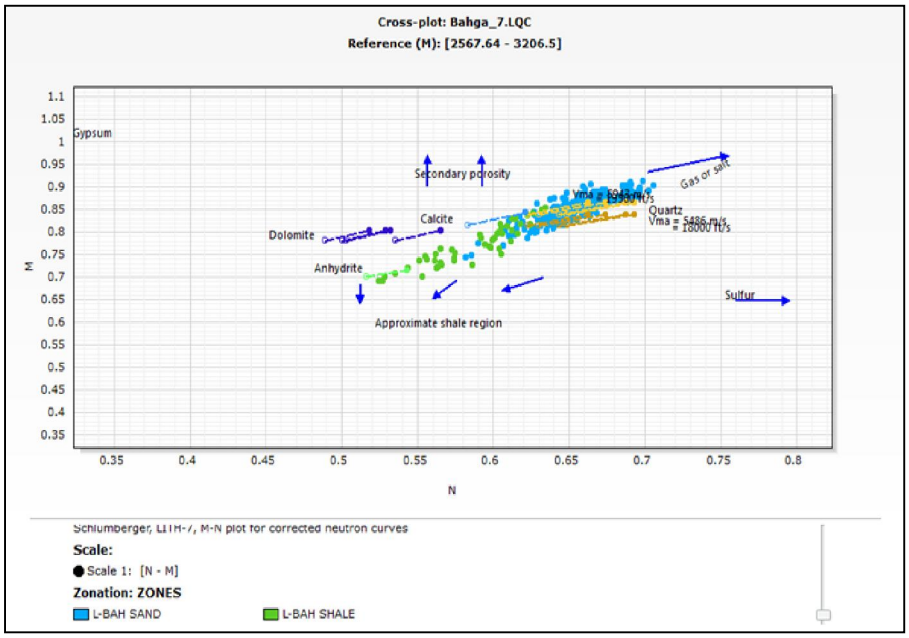

Fig. 11: M-N Cross Plot of Bahga 7, L-BAH.

5.2. Determination of Shale Volume (Vsh):

The shale volume can be calculated either by single-device or combination of two logs (double-device). In the single-device, the shale volume can be calculated through the single log (Gamma ray, self-potential, resistivity, and neutron logs). While in the double- device, the shale volume can be calculated using a combination of dia- porosity device (neutron-density, sonic-neutron, and sonic-density).

According to the shale volume, the rock can be differentiated as:

5.2.1 Single- Curve Indicators

Gamma ray method

It is a very good shale indicator when the radioactivity comes only from shale and the radioactive level of shale in the formation is constant. The shale volume (linear method) calculated according to (Schlumberger, 1972 b) is:

$V_{sh} = [GR_{log} - GR_{min}] / [GR_{max} - GR_{min}]$

Where,

V_{sh}: Shale volume.

GR_{log}: Reading value of gamma ray (API) at the interest interval.

GR_{min}: Reading value of gamma ray (API) at the clean interval.

GR_{max}: Reading value of gamma ray (API) at the shale interval.

Double Curve Shale Indicators

Density-Neutron Method

The shale volume (Vsh) can be estimated by the combination of density and neutron logs using the equation of (Dresser Atlas, 1979) as:- (Vsh) D-N = [A/B]

Where,

A= [pblog (ØNmat – 1.0) – ØNlog (Ømat – pf) – pf (ØNmat + pmat)]

B = [(psh – pf) (ØNmat – 1.0) – (ØNsh – 1.0) (pmat – pf)]

It is affected by the borehole conditions and lithology variation.

This method was used in our study for calculation of the volume of clay from the combination of density and neutron logs using the Duple Clay Indicators work on the principle of defining a clean line through the sandstone reservoir (study area reservoir type) and a clay point. The clay volume is calculated as the distance the input data falls between the clay point and the clean line.

Lithology has been identified from GR, Density/Neutron and PEF log responses. Shale fraction Vsh was calculated using the GR index as a linear response.

Net sand was discriminated from clays using a Vsh cut-off of 50%. Neutron/Density cross-over was also used to eliminate cemented intervals and to provide an indication of uncertainty in the net sand determination.

By applying Techlog Software to calculate the volume of shale Using both single and duple clay indicators, Shale Volume was calculated in the investigated area and it ranges from 18 % in Bahga 1 well to 20 % in Bahga 4 well for AR/G 3, ranges from 9% in Bahga 5 well to 17 % in Bahga 6 well for AR/G 1 and ranges from 23 % in Bahga 3 well to 21 % in Bahga 9 well for L-BAH.

5.3. Determination of Formation Porosity (Φ):

5.3.1 Effective Porosity (Φeff)

The formation porosity can be determined by combining the readings of the two porosity logs. The combination of density and neutron log measurements is probably the most widely used for calculating the true porosity of the formation. The formation porosity can be calculated from a density – neutron combination by using a mathematical equation of Poupon and Gaymard, (1970).

In clean formations:

$$\Phi_{ND} = (\Phi_N + \Phi_D) / 2$$

In shaly formation:

$$\Phi eff = (\Phi_{NC} + \Phi_{DC}) / 2$$

In the presence of gas in the rock pores, the ΦDC will be bigger than ΦNC so the following formula can be used (Schlumberger, 1989):

Different fluid densities (0.8 and 0.9 g/cc) were used to account for different composition of the fluid due to the presence of Oil or water in the logged interval.

The grain density value was taken from the available core data measurements in Bahga field.

The calculated Effective Porosity (Φeff) in the studied wells in the investigated area ranges from 16 % in Bahga 1 well to 18 % in Bahga 4 well for AR/G 3, ranges from 12 % in Bahga 5 well to 17 % in Bahga 6 well for AR/G 1 and ranges from 14 % in Bahga 3 well to 15 % in Bahga 7 well for L-BAH.

5.4 Determination of Fluid Saturation:

The determination of the fluid saturations means principally the differentiation between the various types of fluid components (Water and hydrocarbons).

5.4.1. Water Saturation Determination

Water saturation is the fraction (or percentage) of the pore volume of the reservoir rock that is filled with water or hydrocarbon. Generally in clean or non shaly formation with homogeneous intergranular porosity, the water saturation (Sw) of a reservoir's of the uninvaded zone is calculated by the Archie (1942) equation as follow:

$$S_w = \left(aRw / Rt. \Phi^2 \right)^{1/n}$$

Where,

Sw : Water saturation of the uninvaded zone.

Rw: Resistivity of formation water at formation temperature (Ohm.m)

Rt : True formation resistivity

Φ : Porosity

a : Tortuosity factor = 1

m : Cementation factor = 2

n : Saturation exponent = 2

Calculated water saturation of AR/G 1 in the studied wells in the study area ranges from 12 % in Bahga 5 well to 17 % in Bahga 6 well, AR/G 3 ranges from 29 % in Bahga 1 well to 28 % in Bahga 4 well and L-BAH ranges from 62 % in Bahga 3 well to 32 % in Bahga 9 well.

5.4.2. Hydrocarbon Saturation Determination:

The hydrocarbon saturations were determined as follows:-

Shr = 1 - Sw

Formations water resistivity's (Rw) was taken from the available water samples in Bahga field at AR/G and L-Bahariya and confirmed with Pickett plot. This plots is relation between deep resistivity and porosity to estimate formation water resistivity by select sand body in water leg, Cementation factor and saturation exponent were taken from AR"G" in Bahga 4 SCAL data (Figures 12,13).

5.5. Cut Offs

By applied petrophysical procedures on the TechLog software and get out the cut offs, the average values for petrophysical parameters used in this study include volume of shale, net sand, effective porosity (PHIE), water saturation (Sw), hydrocarbon saturation (Sh) are tabulated in (Table 2). And the histograms of this parameters used in this study include volume of shale, effective porosity and hydrocarbon saturation) for AR/G 1, 3 and L-BAH RES reservoirs are presented in.

Table 1: Sums & Average of Reservoirs Petrophysical Parameters

Well	Zones	N/G	V_{SH}	PHIE	S_W	S_h
Bahga 1	AR/G 1 SAND	0.19	0.06	0.13	0.88	0.12
Bahga 1	AR/G 2 SAND	0.17	0.23	0.15	0.92	0.08
Bahga 1	AR/G 3 SAND	0.40	0.18	0.16	0.29	0.71
Bahga 1	L-BAH SAND	0.11	0.30	0.12	0.96	0.04
Bahga 3	AR/G 1 SAND	0.72	0.15	0.19	0.82	0.18
Bahga 3	AR/G 2 SAND	0.34	0.27	0.16	0.85	0.15
Bahga 3	AR/G 3 SAND	0.04	0.31	0.15	0.84	0.16
Bahga 3	L-BAH SAND	0.65	0.23	0.14	0.62	0.38
Bahga 4	AR/G 1 SAND	0.31	0.11	0.12	0.66	0.34
Bahga 4	AR/G 2 SAND	0.14	0.19	0.15	0.69	0.31
Bahga 4	AR/G 3 SAND	0.73	0.20	0.18	0.28	0.72
Bahga 5	AR/G 1 SAND	0.96	0.09	0.21	0.12	0.88
Bahga 5	AR/G 2 SAND	0.06	0.30	0.15	0.75	0.25
Bahga 5	AR/G 3 SAND	0.35	0.22	0.18	0.57	0.43
Bahga 5	L-BAH SAND	0.33	0.22	0.12	0.80	0.20
Bahga 6	AR/G 1 SAND	0.62	0.17	0.20	0.17	0.83
Bahga 6	AR/G 2 SAND	0.22	0.15	0.16	0.66	0.34
Bahga 6	AR/G 3 SAND	0.77	0.26	0.20	0.52	0.48
Bahga 7	AR/G 1 SAND	0.25	0.13	0.18	0.91	0.09
Bahga 7	AR/G 2 SAND	0.08	0.06	0.15	0.88	0.12
Bahga 7	AR/G 3 SAND	0.08	0.19	0.14	0.83	0.17
Bahga 7	L-BAH SAND	0.77	0.21	0.15	0.64	0.36
Bahga 9	AR/G 1 SAND	0.43	0.15	0.13	0.85	0.15
Bahga 9	AR/G 2 SAND	0.29	0.18	0.15	0.92	0.08
Bahga 9	AR/G 3 SAND	0.30	0.32	0.16	0.9	0.10
Bahga 9	L-BAH SAND	0.32	0.22	0.13	0.31	0.69

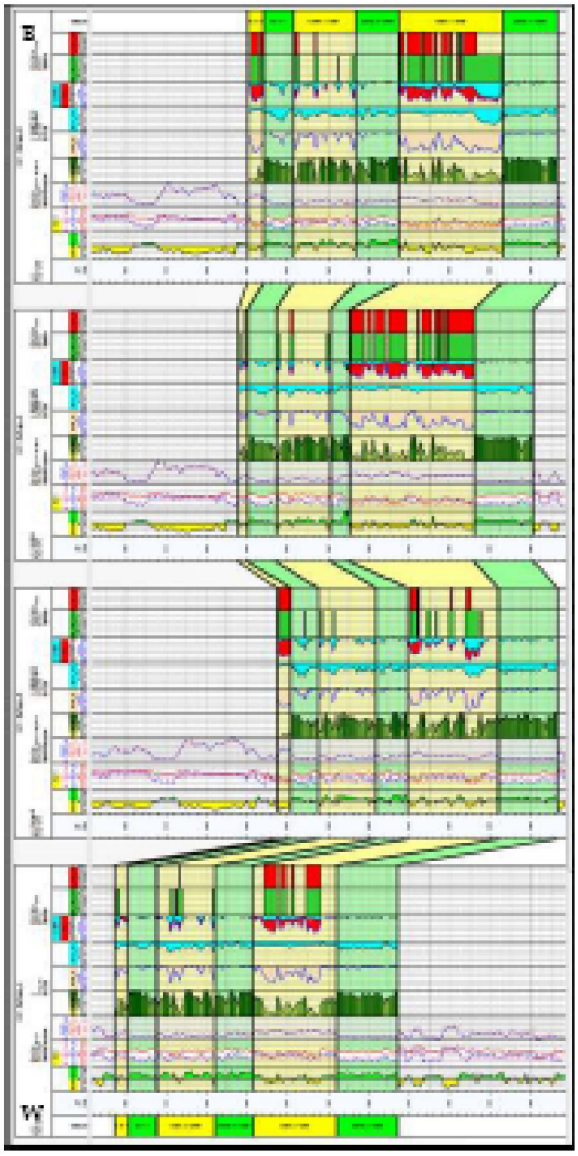

Fig. 12: Correlation of Hydrocarbon Saturation between Bahga 1, 5, 4 and 6 at AR/G.

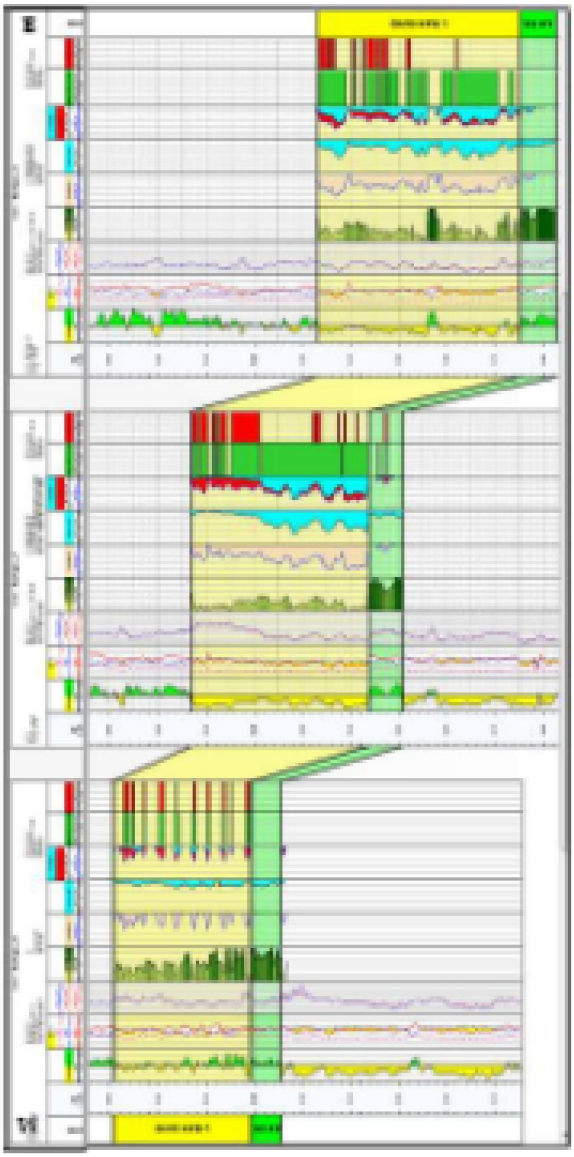

Fig. 13: Correlation of Hydrocarbon Saturation between Bahga 3, 7 and 9 at L-BAH.

6. Illustration of Results

6.1 Vertical Presentation of the Petrophysical Parameters

In order to illustrate the vertical distribution of hydrocarbon saturation through petrophysical parameters, a number of litho-saturation cross-plots were constructed. These plots exhibit a number of continuous logs showing the variations inherited in rocks materials and parameters against depth.

6.1.1 Litho-Saturation Cross-Plots of the Rock Units in Well Bahga 1and 4

Litho-saturation of the rock units of Bahga 1,4 that characterized by predominately shale and sand stone layers. The target at Bahga 1,4 represented in AR/G 3 sand stone layer separated by shale layer.

As illustrated in the computerized litho-saturation cross-plot, Bahga 1,4 of AR/G 3 contains the net sand is 20.7,30.7 meters, the shale content is about 18,20 %, the effective porosity is 16,18 %, and the hydrocarbon saturation is about 70,75 % respectively.

6.1.2 Litho-Saturation Cross-Plots of the Rock Units in Wells Bahga 5and 6

Litho-saturation of the rock units of Bahga 5, 6 that characterized by predominately shale and sand stone layers. The target at Bahga 5, 6 represented in AR/G 1 sand stone layer separated by shale layer.

As illustrated in the computerized litho-saturation cross-plot, Bahga 5, 6 of AR/G 1 contains the net sand

is 3.3,4.2 meters, the shale content is about 9,17 %, the effective porosity is 20,20 %, and the hydrocarbon saturation is about 83,75 % respectively.

6.1.3 Litho-Saturation Cross-plots of the Rock Units in Wells Bahga 3, 7 and 9

Litho-saturation of the rock units of Bahga 3,7,9 that characterized by predominately shale and sand stone layers. The target at Bahga 3,7,9 represented in L-BAH sand stone layer separated by shale layer.

As illustrated in the computerized litho-saturation cross-plot, Bahga 3,7,9 of L-BAH contains the net sand is 41.8, 36.5, 28.5 meters, the shale content is about 23, 20, 22 %, the effective porosity is 14, 15, 13 %, and the hydrocarbon saturation is about 28, 37, 70 % respectively. (Figures 14,15)

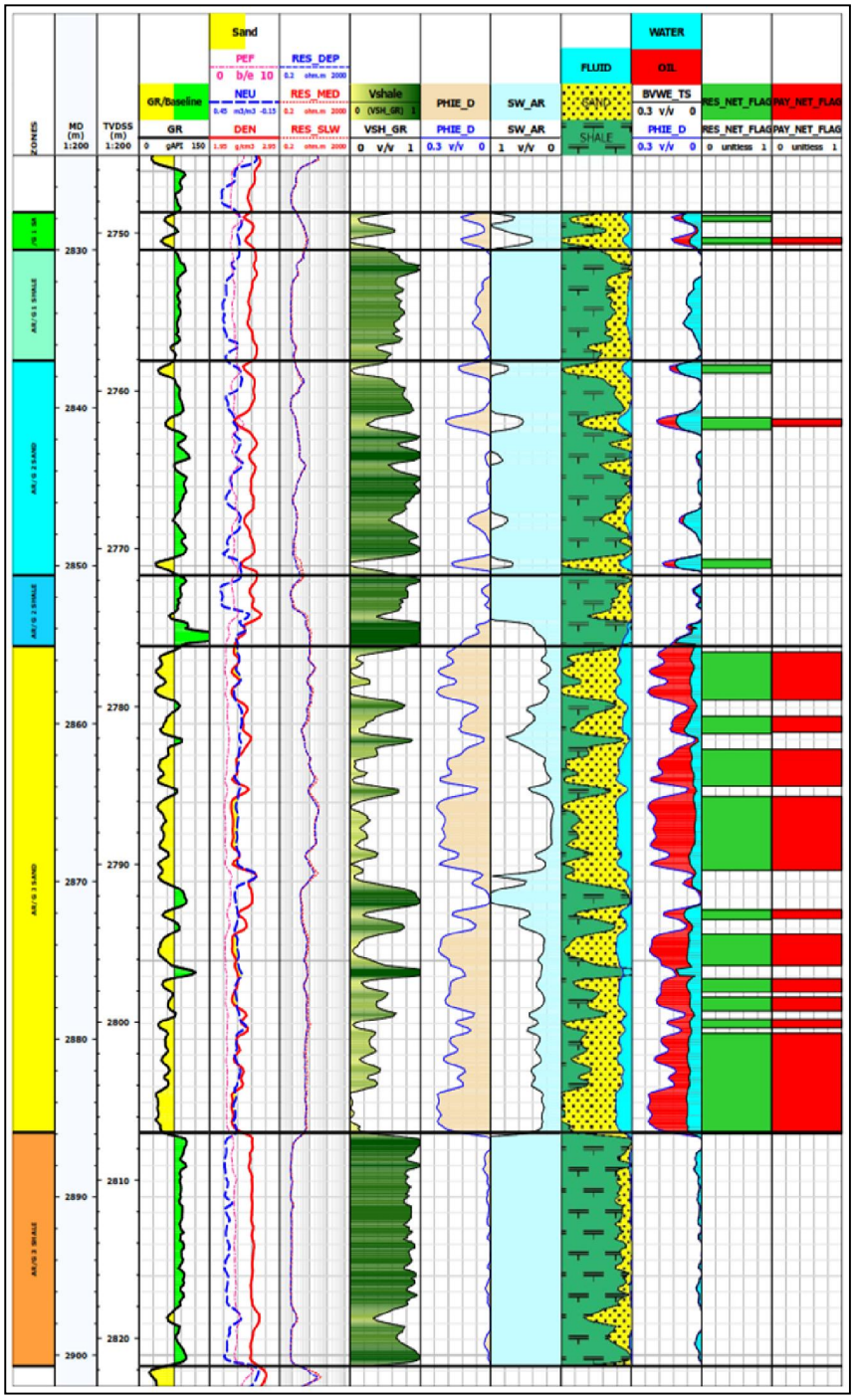

Fig. 14: The Corrected Log Datasets and Litho-Saturation Cross Plot of AR/G 1, 2 and 3 at Bahaga 4.

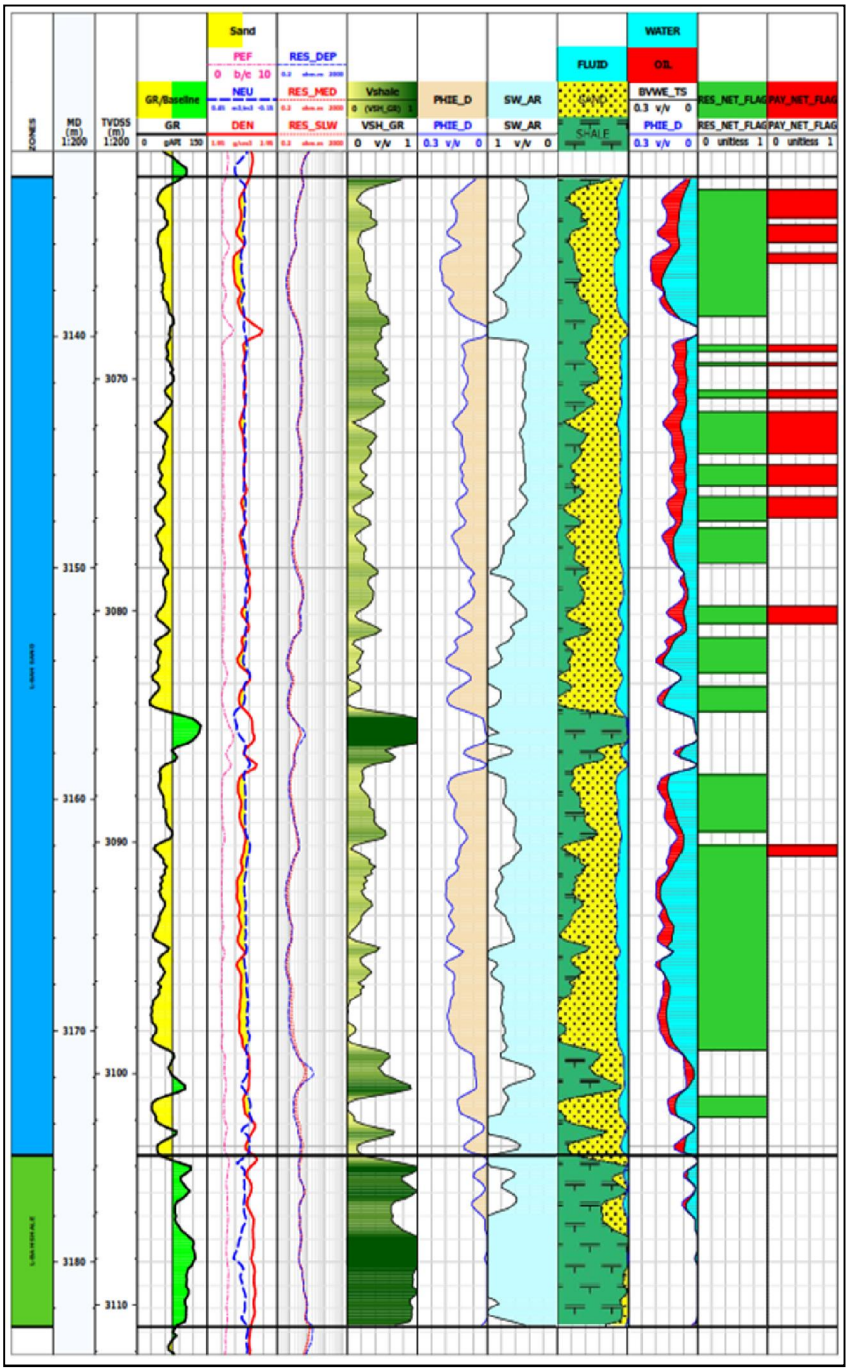

Fig. 15: The Corrected Log Datasets and Litho-Saturation Cross Plot of L-BAH at Bahaga 3.

5.2 Lateral Presentation of Petrophysical Parameters

5.2.1 AR/G 1 Distribution Maps

Four iso-parametric contour maps of AR/G 1 were constructed to illustrate the lateral distribution of the petrophysical parameters in the investigated area.

As presented in (Figures 16-18) for AR/G 1, shale volume decrease, effective porosity increase, hydrocarbon saturation increase toward to eastern part of the Bahga field.

5.2.2 AR/G 3 Distribution Maps

Four iso-parametric contour maps of AR/G 3 were constructed to illustrate the lateral distribution of the petrophysical parameters in the investigated area.

As presented in Figures (19-21) for AR/G 3, shale volume decrease, effective porosity increase, hydrocarbon saturation increase toward to eastern part of the Bahga field.

5.2.3 L-BAH Distribution Maps

Four iso-parametric contour maps of L-BAH were constructed to illustrate the lateral distribution of the petrophysical parameters in the investigated area.

As presented in (Figures 22-24) for L-BAH, shale volume decrease, effective porosity increase, hydrocarbon saturation increase toward to north western part of the Bahga field.

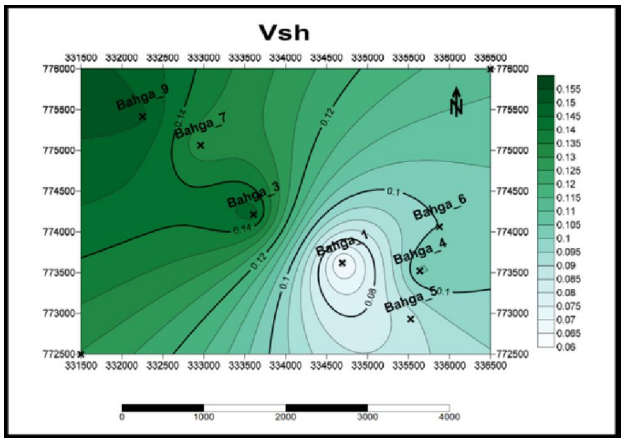

Fig. 16: Distribution Map of shale volume of AR/G 1

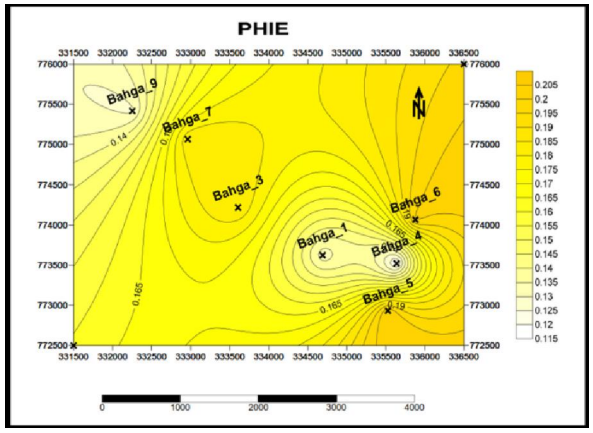

Fig. 17: Distribution Map of Effective Porosity of AR/G 1

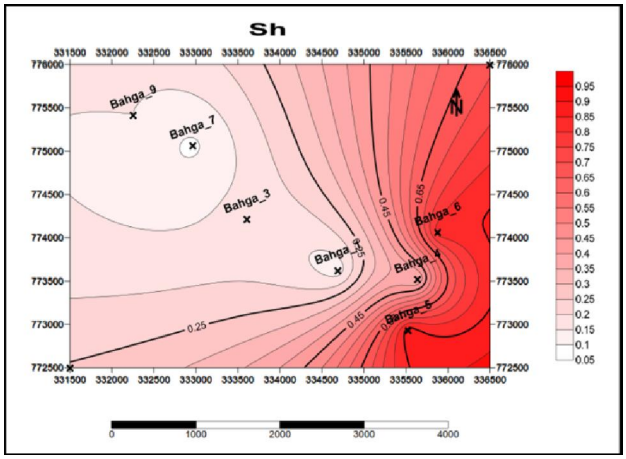

Fig. 18: Distribution Map of Hydrocarbon Saturation of AR/G 1

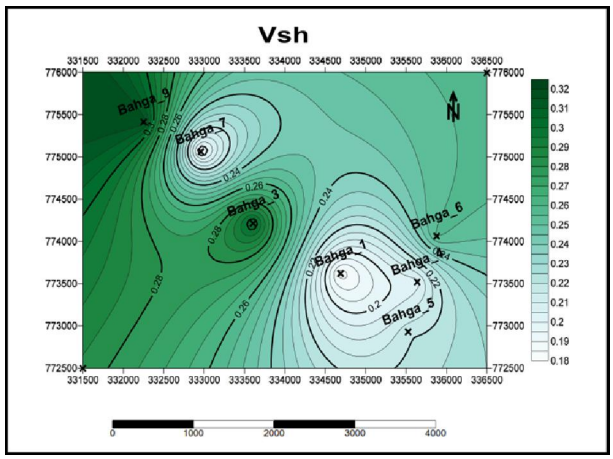

Fig. 19: Distribution Map of shale volume of AR/G 3

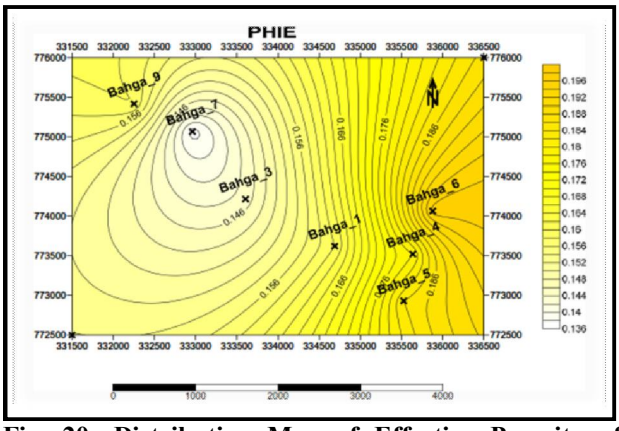

Fig. 20: Distribution Map of Effective Porosity of AR/G 3

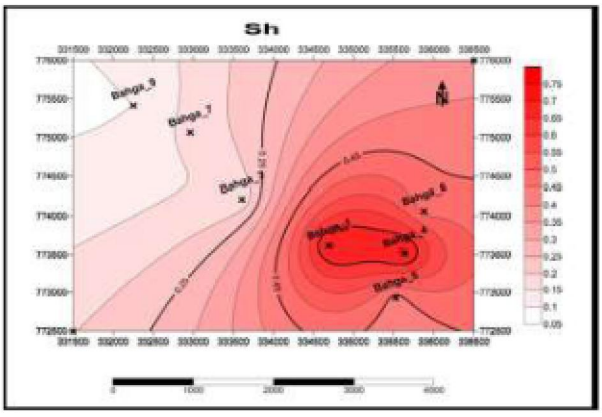

Fig. 21: Distribution Map of Hydrocarbon Saturation of AR/G 3

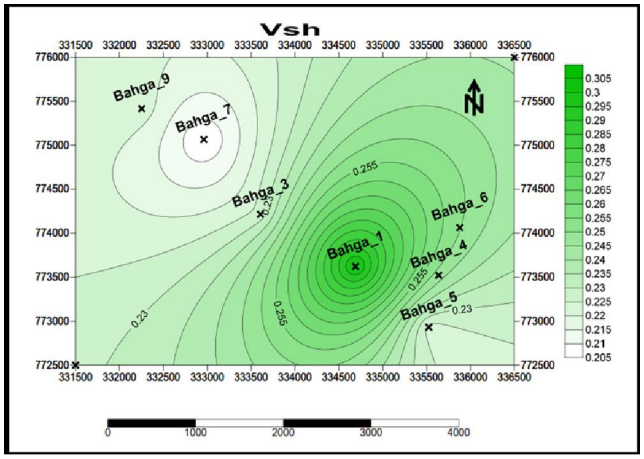

Fig. 22: Distribution Map of shale volume of L-BAH

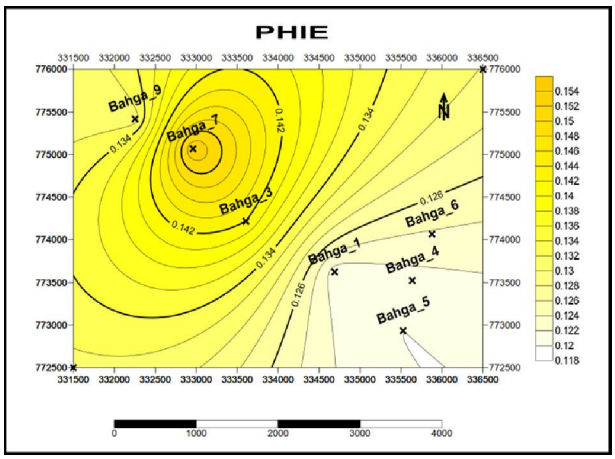

Fig. 23: Distribution Map of Effective Porosity of L-BAH

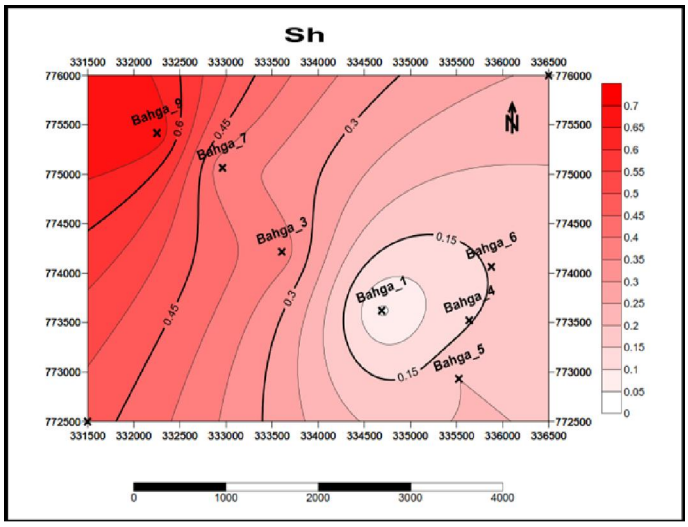

Fig. 24: Distribution Map of Hydrocarbon Saturation of L-BAH

6. Property Modeling

Property modeling processes are used for filling the cells of the grid with discrete (facies) or continuous (petrophysical) properties.

The property modeling process in this study consists of facies well log interpretation for facies modeling where discrete facies are distributed throughout the model grid, well Up-scaling, data analysis and petrophysical modeling.

6.1. Facies Modeling

6.1.1. Facies Model of AR/G SAND 3

AR/G SAND 3 has been subdivided into 20 layers in order to capture the small scale vertical heterogeneity in the appropriate level of details. The nature of the facies AR/G Member is scattered due to the tidal effect. Only in three wells Bahga 1, Bahga 4 and Bahga 6 this zone is characterized by more reservoir sand rather than the other zones.

(Figure 25) shows selective layers at top of AR/G SAND 3 unite, shows that the dominated facies is reservoir sandstone which increases around Bahga 1,4,6 with continue in the east direction and decrease to the north which shaly sand and shale increase.

6.1.2. Facies Model of L-BAH

L-BAH has been subdivided into 30 layers in order to capture the small scale vertical heterogeneity in the appropriate level of details. The nature of the facies L-BAH Member is scattered due to the tidal effect. Only in three wells Bahga 3, Bahga 7 and Bahga 9 this zone is characterized by more reservoir sand rather than the other zones.

(Figure 26) showing selective layers at top of L-BAH member, showing that the dominated facies is reservoir sandstone which increases at the direction of the SW of the area and decrease in the east area where shaly sand and shale increase.

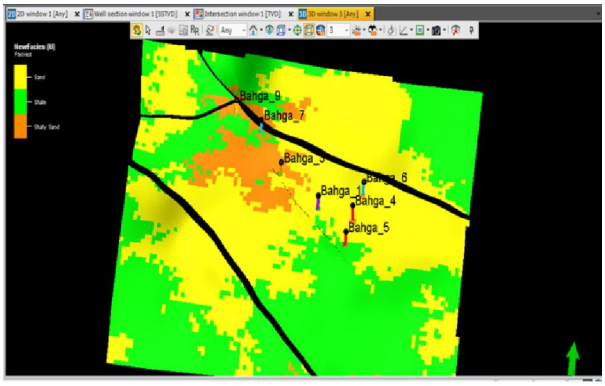

Fig. 25: Selective Facies Layer at Top of AR/G SAND 3

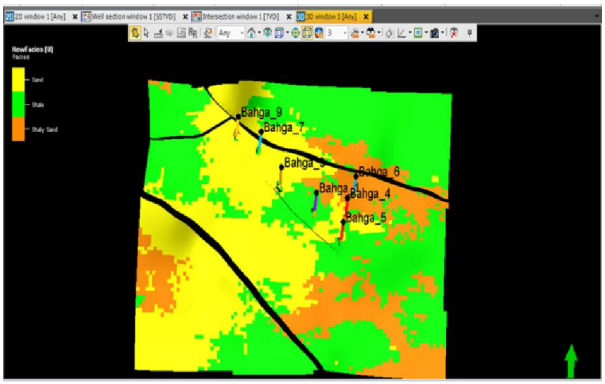

Fig. 26: Selective Facies Layer at Top of L-BAH

6.2. Petrophysical Modeling

Petrophysical modeling is the interpolation or simulation of continuous data (for example, porosity or permeability) throughout the model grid. This is the process of filling the cells of the grid with continuous properties including effective porosity, water and hydrocarbon saturation and shale volume.

In this study PP curves were upscaled and populated using Sequential aussian Simulation for different facies types.

6.2.1 Petrophysical Model of AR/G SAND 3

Figures (27, 28) showing selective layers at the top of AR/G SAND 3 Member and indicate that good effective porosity distribution around Bahga 1, 4 and 6 with low water saturation.

Both effective porosity and water saturation distribution tends to be controlled by facies distribution.

6.2.2 Petrophysical Model of L-BAH

Figures (29, 30) showing selective layers at the top of AR/G SAND 3 Member and indicate that good effective porosity distribution around Bahga 3, 7 and 9 with low water saturation.

Both effective porosity and water saturation distribution tends to be controlled by facies distribution.

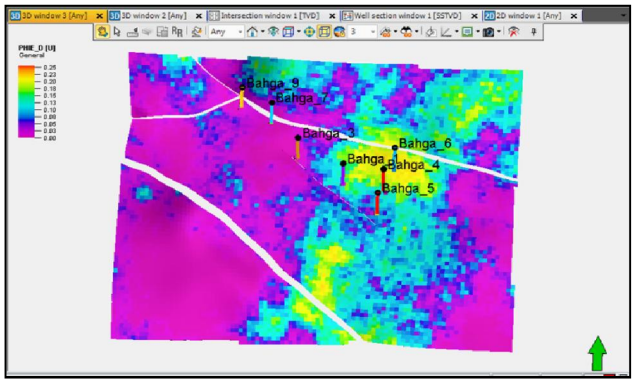

Fig. 27: Model of Effective Porosity Distribution at AR/G SAND 3

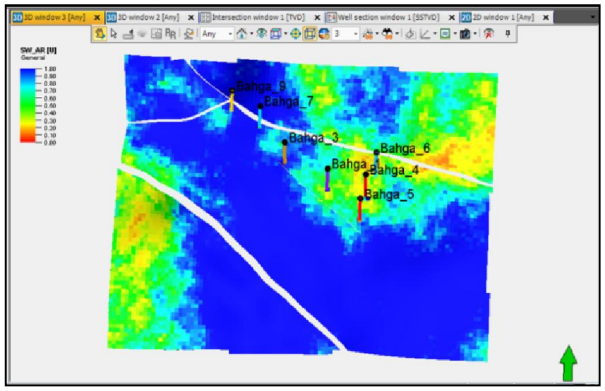

Fig. 28: Model of Water Saturation Distribution at AR/G SAND 3

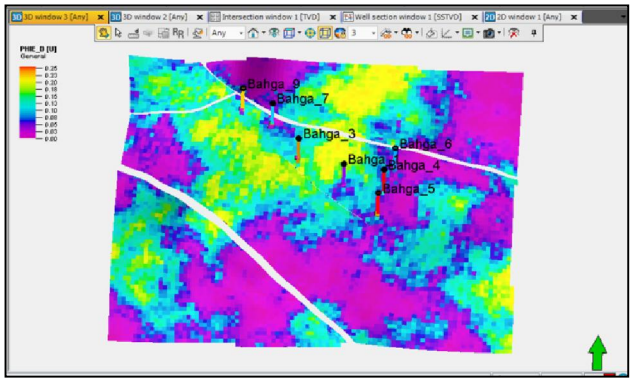

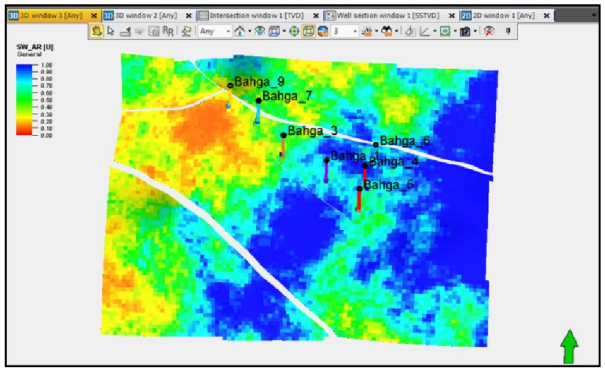

Fig. 29: Model of Effective Porosity Distribution at L-BAH

Fig. 30: Model of Water Saturation at L-BAH

6.3 Prospect Generation and Leads

The intersections of the NW-SE trending faults gave rise to varying structural closures at Bahga field. These closures formed good traps for trapping hydrocarbons in the two main reservoirs (AR/G AND L-BAH members). The structural closures formed in this field mainly three-way closure type. So, from, through interpretation of the seismic sections trends (NW-SE), depth structural contour maps and petrophysical characteristics of Bahga field, depending on the current study a promising area for drilling and development was achieved. According to the present study Bahga field was classified into two closures "A" and "B", the closure "A" area located in the south eastern part, whereas the closure "B" is located in the north western part of this field (Figure 31).

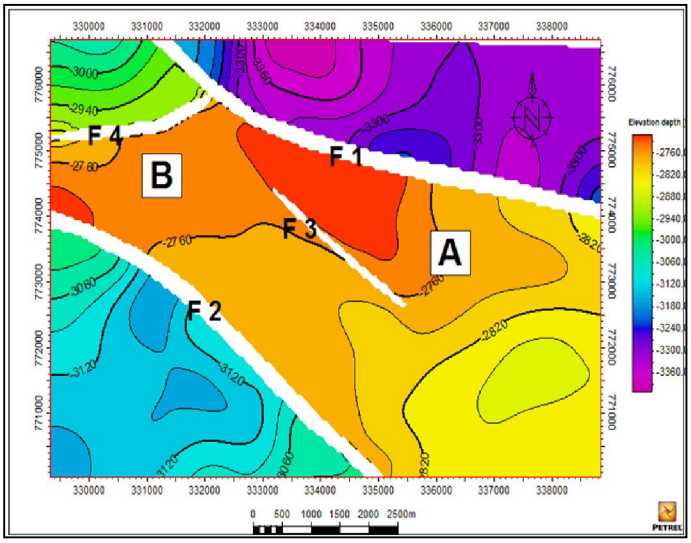

Fig. 31: Structure Contour Map on Top of AR/G Member with the New Prospect Area at Bahga Field.

The new prospect area was selected based on structurally closure, located along the northwest–southeast trending major normal faults number one and two and the good petrophysical characteristics.

7. Summary, Conclusions and Recommendations

The Bahga field lies in the center of the AESW concession, located in the Western desert of Egypt approximately 300 Km to the South West of Cairo.

Only four wells encountered hydrocarbon pay sands in the ARG reservoir (Bahga 1, 4, 5, 6) which are all concentrated in the East of the field outline. The hydrocarbon accumulation in the ARG is delineated by water bearing AR/G sand 2 at all wells in the East and the West and two major faults towards the North and the South.

The upper AR/G reservoir is further divided in zones named AR/G sand 1, 2 and 3. Two vertically separate hydrocarbon oil accumulations have been identified within upper ARG, which are not in pressure communication; AR/G sand 1 and AR/G sand 3.

Only three wells encountered hydrocarbon pay sands in the Bahariya reservoir (Bahga 3, 7, 9) which are all concentrated in the West of the field outline. The Bahariya is divided in three zones; upper Bahariya, intra Bahariya limestone and lower Bahariya.

The main purpose of this study is to evaluate and develop hydrocarbon reservoirs of late cretaceous for AR/G and Bahariya reservoirs at Bahga field that has been done by through studying the following:.

-Seismic Interpretation and 3D Structure Modeling

The manual seismic interpretation of horizons and faults was performed for reservoir sections. The seismic interpretation was set for interpretation for 12 in-lines and 10 cross-line traces with the intention to produce a dense spatial interpretation, for better horizon /surface evaluation needed for modeling the reservoir surfaces.

Manual interpretation is done by petrel software for three horizons, AR/G, BAH and Kharita. The process of generating the faults manually starts by having firm geologic interpretations of the faults, understanding their nature (whether they are planar, listric etc.) and the type of faults. In the Bahga seismic volumes the faults are manually picked within each seismic in-lines and cross-lines in the reservoir sections of the Bahga seismic volumes.

Normally, the seismic interpretation is used to define the main vertical architecture of the reservoir model. When introducing the horizons to the set of pillars generated in the Pillar gridding process, all

intersections between the pillars and the horizons become nodes in the 3D grid.

Finally, 3D structure modeling consists of fault modeling, pillar gridding and vertical layering. All three operation process are tied together one single data model (3D grid).

The field closure is defined primarily by a large bounding fault to the north. Other small-scale, low throw NW-SE trending faults across Bahga Field, run parallel to the main bounding fault along the principal stress direction. The structure is relatively flat to the west, but has a well-defined contour closure to the east.

-Well Log Analysis:

The goal of the evaluation of reservoir properties is the estimation of hydrocarbons in the porous zones encountered in the Late Cretaceous sequence; Abu Roash-G (AR/G) and Bahariya (BAH) Formations from Bahga Field by the seven wells in the study area as revealed by using a computer programs named TechLog. This system was especially developed to perform quantitative estimation for reservoirs in subsurface sequence by using well logs techniques.

Lithology has been identified from GR, Density/Neutron and PEF log responses. Shale fraction Vsh was calculated using the GR index as a linear response. Net sand was discriminated from clays using a Vsh cut-off of 50%. Neutron/Density cross-over was also used to eliminate cemented intervals and to provide an indication of uncertainty in the net sand determination.

Porosity was calculated from the Density log. Different fluid densities (0.8 and 0.9 g/cc) were used to account for different composition of the fluid due to the presence of Oil or water in the logged interval. The grain density value was taken from the available core data measurements in Bahga field.

Water saturation has been calculated using conventional way (Archie's equation) based on density-porosity and deep resistivity logs.

In order to illustrate the vertical distribution of hydrocarbon saturation through petrophysical parameters, a number of litho-saturation cross-plots were constructed. These plots exhibit a number of continuous logs showing the variations inherited in rocks materials and parameters against depth.

AR/G sand 1 is the first target in our study that has found in tow wells; Bahga 5,6 and contains the net sand is 3.3,4.2 meters, the shale content is about 9,17 %, the effective porosity is 20,20 %, and the hydrocarbon saturation is about 83,75 % respectively.

AR/G sand 3 is the second target in our study that found in tow wells; Bahga 1,4 and contains the net sand is 20.7,30.7 meters, the shale content is about 18,20 %, the effective porosity is 16,18 %, and the hydrocarbon saturation is about 70,75 % respectively.

L-BAH is the third target in our study that found in three wells; Bahga 3,7,9 and contains the net sand is 41.8, 36.5, 28.5 meters, the shale content is about 23, 20, 22 %, the effective porosity is 14, 15, 13 %, and the hydrocarbon saturation is about 28, 37, 70 % respectively.

The neutron-density cross plot of AR/G1,2,3 and L-BAH RES of wells_1,4,5,6,3,7,9 (Figs. 4.8 - 4.14) found that the majority of points overlie sandstone line and found that the points around sandstone line and limestone line in addition shows the same clay effect on the plotted data to the bellow right side of the plot.

Using the M-N plot for mineral identification, the lithological content for each zone can be defined with respect to the standard M and N values of the common minerals and rocks in both fresh mud and salt mud filled holes (Schlumberger, 1997).

Points for a mixture of three minerals will be plotted within the triangle formed by lines connecting the three respective single mineral points. Secondary porosity, shaliness and gas-filled porosity will shift the positions of the points with respect to their true lithology and can even mislead the M-N constituents (Schlumberger, 1997).

M-N (Tri-Porosity) Cross-plot indicates that the main component of AR/G 1, AR/G 3 and L-BAH formation is Sandstone represented by Quartz mineral with calcareous cement represented by Calcite and Dolomite minerals.

Four iso-parametric contour maps of AR/G 1, AR/G 3, L-BAH were constructed to illustrate the lateral distribution of the petrophysical parameters in the investigated area.

For AR/G 1 and AR/G 3 found that shale volume decrease, effective porosity increase, hydrocarbon saturation increase toward to eastern part of the Bahga field.

For L-BAH RES found that shale volume decrease, effective porosity increase, hydrocarbon saturation increase toward to western and NW part of the Bahga field.

To confirm that there is a promising area between F1 and F2, 3D facies model and property model have been applied to view the lateral and vertical distribution of the facies and the petrophysical parameters such as the sand net p, porosity, shale content and water saturation.

7.1. Recommendations

As a result of the present study, using the subsurface and Petrophysical evaluation, a new location is proposed to be a prospect area for AR/G is area A and for L-BAH is area B which is located on such a three-way dip closure that is very suitable place for petroleum accumulation.

References

1. Aadland, A.J., and Hassan, A.A. (1972). In Hydrocarbon potential of Abu Gharadig basin in the Western Desert, Egypt (Vol. 81(B3), pp.19). Paper presented at the 8th Arab Petroleum Congress, Algiers.
2. Abd El Aal, A. (1988, November, 20-23). In Structural framework of Abu Gharadig basin Western Desert, Egypt. Paper presented at the 9th Petroleum Exploration and Production Conference, Egyptian General Petroleum Corporation, Cairo. November, 20-23.
3. Abd El Aal, A., and Moustafa, A.R. (1988). In Structral framework of the Abu Gharadig Basin, Western Desert, Egypt (Vol. 2, pp. 23-50). Paper presented at the 9th Exploration and Production Conference, Egyptian General Petroleum Corporation, Cairo.
4. Abd El Kireem, R.M., Schrank, E., Samir, M.A., and Ibrahim, A.I.M. (1996). Cretaceous palaeoecology, palaeogeography and palaeoclimatology of the northern Western Desert, Egypt. 'Review Journal of African Earth Sciences, 22(1), 93-112.
5. Abdel Aal, A., and Mustafa, A. R., 1988 defines Structural framework of the Abu Gharadig basin.
6. Abu El Naga, M. (1984). In Paleozoic and Mesozoic depocenters and hydrocarbon generating areas, northern Western Desert (Vol. 8, pp. 269-287). Paper presented at the 7th Petroleum and Exploration Seminar, Egyptian General Petroleum Corporation, Cairo.
7. Ali, S.M., Besher, G., and Ammar, G. (1989). Razzak oil field stratigraphic study, p. 1-16, GUPCO's internal report, Unpublished (pp. 1-16), GUPCO.
8. Arps, J. J. (1953): The effect of temperature on the density and electrical resistivity of sodium chloride solutions, Trans., AIME, Vol. 198. pp. 327-28.
9. Asquith and Charles, 1982. Well log analysis for geologist. A book published by AAPG, 1982.
10. Ball, J., and Beadnell, H.J. (1903). Bahariya Oasis, its topography and geology, p. 84 (p. 84),Egypt Survey Department.
11. Batman, R.M. and Konen, C.E. (1978): Well site log analysis and the programmable pocket calculator. SPWIL 8th Ann. Log. Symp., Houston, Texas. pp.107-123.
12. Bayoumi, T. (1996). In The influence of interaction of depositional environment and synsedimentary tectonics on the development of some Late Cretaceous source rocks, Abu Gharadig basin, Western Desert, Egypt (Vol. 2, pp. 475-496). Paper presented at the 13th Petroleum Exploration and Production Conference, Egyptian General Petroleum Corporation, Cairo.
13. Blankenhorn, M. (1921). Hunduch der regionalen Geologie Aegypten (Vol. 9). 224 pp., Bd. VII Bull. Inst. Appliedc Geol., 3(2), 16.
14. Dia El Din, M., 1974, worked on Abu Gharadig field Geology.
15. Dolson, C.J., Shaan, V.M., Matbouly, S., Harwood, C., Rashed, R., and Hammouda, H. (2001). The petroleum potential of Egypt. In Downey, W.M., Threet, C. J., Morgan, A. W. (Ed.), Petroleum proviences of the twenty-first century (Vol. Memoir No. 74, p.^pp. 453-482), American Association of Petroleum Geologists, Tulsa, Oklahoma.
16. Dresser Atlas (1979): Log interpretation charts. Dresser Industries Inc., Houston. 107p.
17. Meshref, W.M. (1990). Tectonic framework of Egypt. In Said, R. (Ed.), Geology of Egypt (113-156), Balkema, Rotterdam.
18. Meshref, W.M. (1996). Cretaceous tectonics and its impaction on oil exploration in regional Northern Egypt. 'Review Geol. Soc. Egypt, 2(Spec. Publ.), 199-241.
19. Meshref, W.M., Abu El Karamat, M.S., and El Gindi, M.K. (1988 b). In Exploration concepts for oil in the Gulf of Suez (Vol. 1, pp. 1- 23). Paper presented at the 9th Exploration and Production Conference, Egyptian General Petroleum Corporation, Cairo.
20. Moustafa, A.R., Saoudi, A., Moubasher, A., Ibrahim, I.M., Molokhia, H., and Schwartz, B. (2003): "Structural setting and tectonic evolution of the Bahariya Depression, Western Desert, Egypt".
21. northern African Tethyan margin:an overview. In Macgregor, S.D., Moody, J. T. R., Clark Lowes, D. D. (Ed.), Petroleum geology of North Africa (Vol. Special Publication No. 132, pp. 217–229, Geological Society, London.
22. Paleoservice. (1986). The hydrocarbon potential of the Paleozoic rocks of the Western Desert, Egypt.
23. Pirson, S.J., 1963: handbook of well log analysis for oil and gas formation evaluation. Pretice hall Inc. Englewood Cliffs P.P 326.
24. Poupon A and Gaymard R, 1970. The evaluation of clay content from logs. SPWLA 11th Annual Logging Symposium, Conference paper: 1970-G.
25. RRI. (1982). Petroleum potential evaluation of the Western Desert, Egypt, p. Unpublished report prepared for EGPC (p. Unpublished report prepared for EGPC), Robertson Research International Limited.
26. RRI. (1985). Further evaluation of the Abu Sennan–Alam El Shawish area, Western Desert, the Arab Republic of Egypt, with emphasis on

stratigraphic trapping potential, Robertson Research International Limited.
27. Said R., 1990, worked on geology of Egypt. Salah, M., and Paradisi, C., 1992, worked on BHI applications.
28. Said, R. (1962). Geology of Egypt. 377 pp. Amsterdam, Elsevier Science Publishing Company Inc.
29. Schlumberger (1972): The essential of log interpretation practice. Schlumberger Ltd., France, pp. 45-67. Schlumberger (1974): Log interpretation manual: Vol. II (Application), Schlumberger Limited, New York, 116p.
30. Schlumberger (1974): Log interpretation manual: Vol. II (Application), Schlumberger Limited, New York, 116p.
31. Schlumberger (1987): Log interpretation, Principles/Applications. Schlumberger Educational Service, Houston, Texas 77010, USA, 189p.
32. Schlumberger (1995): Well evaluation conference of Egypt. Schlumberger technical editing services, Chester. 356 p.
33. Schlumberger (1997): Log Interpretation Charts, Schlumberger, Well services. Pans, France.
34. Schlumberger (2004): Intractive Petrophysics software, operating manual, Version 3.1.
35. Schlumberger Educational Services, 1989, "Formation MicroScanner Image Interpretation," Catalog No. SMP-7028.
36. Schlumberger, 1984. Egypt Well Evaluation Conference (WEC), Cairo, Egypt. Smith, Ch. M., (editor).
37. Sestini, G. (1984): Tectonic and sedimentary history of the NE Africa margin (Egypt - Libya) In Dixon, E.J., Robertson, F. H. A. (Ed.), the geological evolution of the Eastern Mediterranean pp.161175, Blackwell Scientific Publications, Oxford.
38. Sestini, G. (1995): Egypt. In Kulke, H. (Ed.), Regional petroleum geology of the world, part II: Africa, America, Australia and Antarctica (Vol. Beitrنge zur regionalen Geologie der Erde, Band 22, pp. 66-87),
39. Shackleton, R.M. (1980). Precambrian tectonic of NE Africa. 'Review Bull. Inst. Appliedc Geol., 3(2), 16.
40. Soliman, S.M., and El Badry. (1980). Nature of Cretaceous sedimentation in the Western Desert, Egypt. 'Review American Association of Petroleum Geologists Bulletin, 34(12), 2349-2370.
41. Wasfi et al (1986), Bayoumi, T., and Mahmoud, A., 1992, Bayoumi, T., 1994, Bakry, G., 1994, Hassouba, M., 1995, Essam, M., et al., 2013 worked on stratigraphy of Abu Roash"C" and "G reservoirs in Abu Gharadig basin.
42. Worthington, P.F., (1985): Evaluation of shaly-sand concepts in reservoir evaluation. Log Analyst. 26. PP 23-40.

11/20/2017